Accepted to ApJ

HST/STIS Ultraviolet Spectroscopy of the Components of the Massive Triple Star δ Ori A[1]

Noel D. Richardson, Anthony F. J. Moffat

Département de physique and Centre de Recherche en Astrophysique du Québec (CRAQ), Université de Montréal, C.P. 6128, Succ. Centre-Ville, Montréal, Québec, H3C 3J7, Canada;
richardson@astro.umontreal.ca, moffat@astro.umontreal.ca

Theodore R. Gull, Don J. Lindler

Astrophysics Science Division, NASA Goddard Space Flight Center, Greenbelt, MD 20771, USA;
theodore.r.gull@nasa.gov, don.j.lindler@nasa.gov

Douglas R. Gies

Center for High Angular Resolution Astronomy and Department of Physics and Astronomy, Georgia State University, P. O. Box 5060, Atlanta, GA 30302-5060, USA;
gies@chara.gsu.edu

Michael F. Corcoran

CRESST and X-ray Astrophysics Laboratory NASA/GSFC, Greenbelt, MD 20771, USA; Universities Space Research Association, 7187 Columbia Gateway Drive, Columbia, MD 21046, USA;
michael.f.corcoran@nasa.gov

André-Nicolas Chené

Gemini Observatory, Northern Operations Center, 670 North A'ohoku Place, Hilo, HI 96720, USA;
achene@gemini.edu

ABSTRACT

The multiple star system of δ Orionis is one of the closest examples of a system containing a luminous O-type, bright giant star (component Aa1). It is

often used as a spectral-type standard and has the highest observed X-ray flux of any hot-star binary. The main component Aa1 is orbited by two lower mass stars, faint Aa2 in a 5.7 day eclipsing binary, and Ab, an astrometric companion with an estimated period of 346 years. Generally the flux from all three stars is recorded in ground-based spectroscopy, and the spectral decomposition of the components has proved difficult. Here we present HST/STIS ultraviolet spectroscopy of δ Ori A that provides us with spatially separated spectra of Aa and Ab for the first time. We measured radial velocities for Aa1 and Ab in two observations made near the velocity extrema of Aa1. We show tentative evidence for the detection of the Aa2 component in cross-correlation functions of the observed and model spectra. We discuss the appearance of the UV spectra of Aa1 and Ab with reference to model spectra. Both stars have similar effective temperatures, but Ab is fainter and is a rapid rotator. The results will help in the interpretation of ground-based spectroscopy and in understanding the physical and evolutionary parameters of these massive stars.

Subject headings: stars: individual (δ Ori) — stars: binaries: spectroscopic — stars: binaries: visual — ultraviolet: stars

1. Introduction

The western-most of the three stars in the "Belt of Orion" is the multiple star system δ Orionis (Mintaka; HD 36486), and the brightest component of the system represents one of the nearest of the luminous O-type stars (O9.5 II Nwk; Sota et al. 2011). The system consists of a close eclipsing pair Aa1,Aa2 that is orbited by Ab with a current angular separation of $0\farcs3$ (Tokovinin et al. 2014), and there are two other more distant components B and C (Harvin et al. 2002). The system was the target of a recent multiwavelength observing campaign to explore its X-ray properties (Corcoran et al. 2015; Nichols et al. 2015), photometric and spectroscopic variability (Pablo et al. 2015), and spectral properties (Shenar et al. 2015). These studies depend on stellar parameters of the O-star and its close companions, and there remains some confusion about the nature of the companions because the flux of all three stars is generally recorded in observations with limited angular resolution. The single-lined spectroscopic orbit of the O-star (component Aa1) is well established (Harvey et al.

[1]Based on observations made with the NASA/ESA Hubble Space Telescope, obtained at the Space Telescope Science Institute, which is operated by the Association of Universities for Research in Astronomy, Inc., under NASA contract NAS 5-26555. These observations are associated with program #13450.

1987), but attempts to find and measure the Doppler shifts of its companion Aa2 have led to different conclusions. Harvin et al. (2002) analyzed the available collection of ultraviolet spectra from the *International Ultraviolet Explorer* satellite, and they fit cross-correlation functions of the observed spectra with that of a sharp-lined template star to determine a double-lined solution that led to relatively small mass estimates. Mayer et al. (2010) presented a study of the light curve and high S/N optical spectra, and they argued that the spectral signature of the Ab component was significant while that from Aa2 was too faint to detect. They suggested that the light and radial velocity curves of the Aa1,Aa2 binary were consistent with the masses expected for their spectral classifications. Harmanec et al. (2013) extended this work to search for evidence of the Aa2 spectral component in a large set of spectra recording the He I λ6678 absorption line, and their spectral reconstruction methods detected the faint companion signal with an orbital semiamplitude of $K_2 = 273$ km s^{-1} (leading to a mass ratio $q = 0.40$). The conclusions of Mayer et al. and Harmanec et al. are generally verified in the recent orbital analysis by Pablo et al. (2015) and the spectral investigation by Shenar et al. (2015). The stellar properties of δ Ori are consistent with its membership in the Ori OB1b association (at a distance of 380 pc for the nearby σ Ori cluster; Caballero & Solano 2008), which is about twice as far as estimated by the *Hipparcos* parallax (Shenar et al. 2015).

The most direct solution to the problem of the spectral identities of the stars is to obtain angularly resolved spectroscopy of the Aa and Ab components separately. Here we present the first direct resolution of the spectral components through ultraviolet (UV) spectroscopy with the Space Telescope Imaging Spectrograph (STIS) aboard the *Hubble Space Telescope*. We describe in §2 the STIS observations made during two visits that occurred near the times of the velocity extrema of the Aa1,Aa2 binary system. We used cross-correlation methods to measure the radial velocities of Aa1 and Ab that we present in §3. Average versions of the UV spectra of Aa1 and Ab are compared with model spectra in §4 in order to estimate their effective temperatures and projected rotational velocities. We summarize our results in §5 and discuss how they may be used to analyze spectra that record the flux of all three stars.

2. Spectroscopic Observations

The STIS UV spectra of δ Ori were obtained during visits on 2014 Dec 30 and 2015 Feb 10, which correspond to times near Aa1 radial velocity maximum and minimum, respectively, based upon the ephemeris of Mayer et al. (2010). We used the E140M echelle grating that records the UV spectrum over the range 1144 to 1730 Å with a spectral resolving power

of $R = \lambda/\triangle\lambda \sim 46000$ (Kimble et al. 1998; Biretta et al. 2015). The 0.3X0.05ND slit was oriented with the long axis approximately perpendicular to the position angle between Aa and Ab in order to minimize any flux contamination from the other star at 0.″3 separation. The alternative of placing both stars on the slit is impractical because of the close spacing of the echelle orders on the MAMA detector. We expect that at this separation the intensity from the respective companion will be reduced by about 400× its peak value according to the spatial point spread function (PSF) for the FUV-MAMA detector (Biretta et al. 2015). A first exposure of Aa of 300 s duration was made before moving to Ab for a longer exposure of 1360 s. The spatial profile of the Aa spectrum appeared double-peaked in data from the first visit, while the spatial distribution of the Ab spectrum appeared double-peaked in the data from the second visit. We suspect that this anomaly resulted from tracking errors related to the guide stars used in these observations. This has no impact on the wavelength calibrations and relative spectral fluxes of the individual observations. Note that the narrow width of the aperture subsamples the PSF of *HST*, and small variations due to thermal shifts of focus contribute to changes in the flux throughput. Thus, our observations are not well suited to estimate the absolute flux calibrations of the spectra. For example, we find that the mean flux ratio in the region near 1319 Å is $F_\lambda(\mathrm{Ab})/F_\lambda(\mathrm{Aa}) = 0.38$ and 0.26 for the first and second visits, respectively, which is a much larger variation than expected for the orbital light curve (Pablo et al. 2015).

The STIS spectra were extracted and calibrated using the standard STScI pipeline (Bostroem & Proffitt 2011). The final product is a `x1d.fits` file of absolute flux as a function of heliocentric wavelength for each echelle order. We transformed these onto a standard wavelength grid in increments of $\log\lambda$ equivalent to a pixel step of 10 km s^{-1}. This was accomplished by forming the error weighted mean for each wavelength bin from all the available input data (including points from adjacent orders). This resulted in a slight degradation of the resolving power but an increase in the net signal-to-noise ratio, reaching a value of $S/N \approx 30$ per pixel in the best exposed parts of the spectrum. There were some small gaps in wavelength coverage between a few orders long-ward of 1680 Å, and the spectrum was interpolated in wavelength for those missing wavelength bins. Each spectrum was normalized by a second order fit of the fluxes. The UV spectrum of δ Ori is inscribed with a rich collection of interstellar lines, and most of these were removed by direct interpolation across the features so that their impact is minimal in the following treatment of the stellar spectra.

3. Radial Velocities and Orbital Elements

We measured radial velocities for each of the Aa1 and Ab spectral components by calculating the cross-correlation function (CCF) of the observed spectrum with a model template. The models were formed by interpolation in the OSTAR2002 grid of synthetic spectra[2] from Lanz & Hubeny (2003). These models are based upon line-blanketed, non-LTE stellar atmospheres for static photospheres, so they do not include the wind features found in luminous star spectra. In fact, the wind lines display minimal orbital motion because much of the line formation occurs far from the star where the motion is primarily radial, so the wind line regions were excluded in the CCF calculation (omitting the entire low wavelength range 1150 – 1249 Å and the regions surrounding Si IV λ1400 and C IV λ1550). The rotationally broadened model spectra were selected using the stellar parameters for Aa1 and Ab derived by Shenar et al. (2015). The resulting CCFs for Aa1 and Ab are illustrated in the left and right panels, respectively, of Figure 1. Component Ab appears to be radial velocity constant between the observations, as expected for its long orbital period ($P = 346$ y; Tokovinin et al. 2014). However, component Aa1 shows the Doppler shifts corresponding to its orbital motion in the close binary. Noteworthy by its absence is any indication of a signal in the CCF from the Aa2 companion, which is probably due to its relative faintness. We derived radial velocities by fitting a parabola to the peak of the CCF, and these velocities are listed in Table 1. Table 1 gives the component identification, the heliocentric Julian data at the time of mid-exposure, the orbital phase relative to phase zero at eclipse minimum (Pablo et al. 2015), the radial velocity, and its uncertainty (from analytic estimates using the method of Zucker 2003).

The lack of evidence of Aa2 in the CCFs presented in Figure 1 clearly indicates that it contributes only a small fraction of the UV flux. We attempted a search for its spectral contribution by considering the difference spectrum of our two quadrature observations of Aa. Both flux normalized spectra of Aa were shifted to the rest frame of Aa1 using the measured velocity shifts in Table 1, and then the second spectrum was subtracted from the first to remove most of the contribution of Aa1. The resulting difference spectrum will also be equal to the residual spectrum of Aa2 at its blueshifted position in the first spectrum minus that for its redshifted position in the second spectrum. Thus, we might expect that the CCF of this difference spectrum would display a blueshifted peak (correlation with the absorption lines in the first spectrum) and a redshifted trough (anticorrelation with the reversed absorption lines in the second spectrum). We calculated several model template spectra for Aa2 using stellar parameters close to those found by Shenar et al. (2015) with models from the BSTAR2006

[2]http://nova.astro.umd.edu/

grid of Lanz & Hubeny (2007), which cover the lower temperature range expected for Aa2. The best correlation was obtained with selected values of $T_{\rm eff} = 23$ kK, $\log g = 4.0$, and $V \sin i = 40$ km s^{-1}. The latter was chosen from the widths of the peaks in the CCF when a $V \sin i = 0$ model was used as a template. The projected rotational velocity of Aa2 is smaller than that found by Shenar et al. $V \sin i = 150 \pm 50$ km s^{-1}, but the disagreement is not surprising given that Shenar et al. obtained their measurement from a difficult blend analysis of the weak line wings of He I $\lambda\lambda 4026, 4144$ (see their Fig. 4). The CCF of the difference spectrum and the model is shown in Figure 2. This CCF is clearly dominated by noise in the difference spectrum, but there does appear to be a peak and a trough at the velocities relative to the Aa1 frame that should correspond to the Doppler shifts of Aa2. There is also a weaker peak at zero velocity that is associated with the lingering presence of the features of Aa1 in the difference spectrum. We made parabolic fits of the positions of the peak and trough extremities (indicated by the dotted lines in Fig. 2), and these velocities were added to the Aa1 velocities to yield the heliocentric system velocities reported in Table 1. Because this is a tentative detection, we simply estimated the uncertainties as 0.5× HWHM of the peak and trough distributions in the CCF.

We can compare these velocity measurements for Aa1 with the recent orbital solution from a large set of contemporaneous, ground-based spectroscopy presented by Pablo et al. (2015). We began by assuming the period P from the work of Mayer et al. (2010) and the epoch of periastron T, eccentricity e, and longitude of periastron ω from the "LM" (low mass) solution of Pablo et al. (2015). We then adopted the rate of periastron advance derived by Pablo et al. to prorate T and ω to the periastron that occurred at the mean time of our observations (130 orbital cycles after the periastron epoch given by Pablo et al.). We are then left with two radial velocities to find the remaining two orbital elements, the systemic velocity γ and the semiamplitude K. In such a situation, we cannot estimate parameter uncertainties from the residuals to the fit, because the residuals are zero, so we simply set the errors in these two parameters equal to the mean error of the velocities. We used the program described by Morbey & Brosterhus (1974) to find the values of γ_1, γ_2, K_1, and K_2 that are listed in Table 2. Our estimate of γ_1 is intermediate between those determined by Mayer et al. (2010) and Pablo et al. (2015), and small differences in systemic velocity are not unexpected given the different methods of radial velocity measurement. Our derived value of $K_1 = 104.6 \pm 1.6$ km s^{-1} falls between those found by Pablo et al. (2015) and Harmanec et al. (2013), $K_1 = 96.0 \pm 0.6$ and 109.0 km s^{-1}, respectively. Our estimate of $K_2 = 266 \pm 20$ km s^{-1} agrees within uncertainties with that found by Harmanec et al. (2013), $K_2 = 273$ km s^{-1}.

The mass ratio we derive from our tentative detection of the CCF signal of Aa2, $q = M_2/M_1 = 0.39 \pm 0.03$, is consistent with estimates from the eclipsing light curve (Luyton

et al. 1939; Koch & Hrivnak 1982; Mayer et al. 2010; Pablo et al. 2015). Table 2 lists the resulting masses for Aa1 and Aa2 that we derive using an orbital inclination $i = 76\overset{\circ}{.}3$ from Pablo et al. (2015). Both stars have masses in line with expectations from their temperatures and luminosities (Martins et al. 2005; Torres et al. 2010), and our work confirms that the lower masses found by Harvin et al. (2002) resulted from an incomplete treatment of the spectral signature of component Ab. The mass of the entire triple system derived from the preliminary astrometric orbit (Tokovinin et al. 2014) is $40M_{\odot}(d/400\ \mathrm{pc})^3$ where d is the distance to the Ori OB1b association in which δ Ori resides. The difference between the total mass and the Aa masses in Table 2 would imply that the mass of Ab is only $8M_{\odot}$, much lower than the $22M_{\odot}$ mass estimated by Shenar et al. (2015) for a star of its effective temperature and luminosity. We suspect that future revisions to the astrometric orbit of Aa,Ab may well change this low mass estimate.

4. Spectral Properties

The excellent quality of the STIS spectra of components Aa1 and Ab encouraged us to compare their spectral morphology to model spectra in order to make independent estimates of the stellar parameters. We formed a simple shift-and-add average of the Ab spectra to move them to the rest frame. We did the same for the Aa1 spectra (using the velocities in Table 1), but the results are marred in the vicinity of the wind lines because they do not exhibit orbital motion. Instead, we made a simple mean spectrum (shifted to the rest frame using γ_1) to represent the spectrum of Aa1 in spectral regions near the wind features of C III λ1175, Lyα λ1216, N V λ1240, Si IV λ1400, and C IV λ1550. Figure 3 shows the two versions of the Aa1 spectrum using black plus signs for the shift-and-add average of the photospheric parts and using gray crosses for the simple average applied to the wind line regions. Figure 4 likewise illustrates the average spectrum of component Ab. Both figures are marked by small vertical ticks near the bottom that indicate the positions of the interstellar lines that were removed. The spectra of Aa1 and Ab shown in Figures 3 and 4 are available as FITS files attached to the electronic version of this paper.

We formed model spectra using the OSTAR2002 grid from Lanz & Hubeny (2003). These are based on the line-blanketed and non-LTE atmosphere code TLUSTY and spectrum synthesis code SYNSPEC, and the model spectra we used have solar metallicity and an adopted microturbulent velocity of 10 km s^{-1}. We made a bilinear interpolation in $(T_{\mathrm{eff}}, \log g)$ to derive a flux model, and then the fluxes were rebinned on the $\log\lambda$ grid of the STIS observations. The model spectra were convolved with a rotational broadening function using an assumed value of projected rotational velocity $V \sin i$ and a linear limb darkening

coefficient from the tables of Wade & Rucinski (1985).

We began by exploring the photospheric line broadening in the spectra of Aa1 and Ab. We derived a $V \sin i = 0$ model spectrum, and then compared rotationally convolved versions of the model over a grid of $V \sin i$ values and for series of ≈ 50 Å regions across the spectrum that were free of wind features. The resulting $V \sin i$ value and its standard deviation are reported in Table 3 for components Aa1 and Ab. We also list there an estimate of $V \sin i$ for Aa2 based on the width of the its CCF peak in Figure 2. Our $V \sin i$ values for Aa1 and Ab are $\approx 13\%$ larger than those given by Shenar et al. (2015), because Shenar et al. attributed part of the line broadening to macroturbulence. Component Ab is clearly a rapidly rotating star, and its spectral line profiles are broad and shallow. Furthermore, its flux ratio in the V-band is $F_\lambda(\mathrm{Ab})/F_\lambda(\mathrm{Aa}) = 0.28$ (Mason et al. 2009), so its flux contribution cannot be ignored in radial velocity studies of ground-based spectroscopy. These factors are the main reasons why it is has been so difficult to sort out the different component contributions in the past (Mayer et al. 2010).

We next considered the best fit $T_{\rm eff}$ models that match the UV spectra of Aa1 and Ab. We formed a grid of models around the expected temperatures and convolved these with the respective rotational broadening functions. Because the main luminosity criteria in the UV spectra involve the wind lines and the TLUSTY models do not account for the wind, we chose to set the gravity $\log g$ (the atmospheric parameter related to radius) to the estimates given by Shenar et al. (2015) for $\log g_{2/3}$ (the gravity at optical depth $\tau_{\rm Ross} = 2/3$). The model spectra were rectified in the same way as the observations by dividing by a second order polynomial fit of the relatively line-free regions. We formed a χ^2 statistic of the observed and model spectral differences over those regions of the spectra free of wind lines, and then we estimated the temperature that minimized χ^2. Our temperature results appear in Table 3. Although the derived values of $T_{\rm eff}$ are similar for both Aa1 and Ab, we find that Ab is the hotter star by a small margin. Our estimates are about 7% hotter than those found by Shenar et al. (2015), but there are several explanations for this difference. First, Shenar et al. used optical lines of He I and He II as the primary temperature diagnostics, while our results are based on the ultraviolet metallic lines. Heap et al. (2006) found that $T_{\rm eff}$ estimates from optical lines led to lower temperatures than those from UV lines in their analysis of some O-star spectra, so Aa1 and Ab may represent additional cases that show a systematic offset. Second, the $T_{\rm eff}$ result is sensitive to the adopted gravity. For example, a smaller $\log g$ will result in a lower $T_{\rm eff}$ in order to match the observed ionization ratios of the lines. If we had adopted lower values from Shenar et al. of $\log g = \log g_{\rm eff} = \log g_\star (1 - \Gamma)$, i.e., the gravity corrected for the outward radiative force, then our resulting $T_{\rm eff}$ would be closer to their values. Third, the UV metallic line strengths will increase with increasing microturbulent velocity (Heap et al. 2006). Shenar et al. derived microturbulent velocities

of $\xi_{\rm ph} = 20 \pm 5$ and 10 ± 5 km s^{-1} for Aa1 and Ab, respectively, so it is possible that we arrived at a hotter $T_{\rm eff}$ for Aa1 by incorrectly adopting $\xi_{\rm ph} = 10$ km s^{-1} in a solution that relied heavily on the strengths of Fe V lines that locally increase in strength with higher $T_{\rm eff}$. Fourth, the model spectra are based on the assumption of spherical stars, whereas Aa1 and especially Ab will have an oblate shape due to their rotation. The local temperature, gravity and specific intensity will decrease from pole to enlarged equator, so that the UV results may preferentially represent conditions closer to the hotter poles than those from optical spectra.

The final model spectra are shown as solid lines in Figures 3 and 4. The fit is quite satisfactory across the UV spectrum with the obvious exception of the strong stellar wind lines in Aa1 that are absent in the TLUSTY models. Shenar et al. (2015) have made good fits of the UV wind lines of Aa1 using their PoWR atmospheres code. The wind features of Ab, on the other hand, appear similar to the photospheric predictions, which probably indicates that Ab is a lower luminosity star (dwarf or giant).

5. Summary

The exquisite angular resolving power of STIS has allowed us to separate the spectra of δ Ori Aa and Ab for the first time. The results verify that Ab is indeed a hot, rapidly rotating star that is a significant flux contributor across the spectrum. It will be important to continue angular measurements of its orbit in order to determine its mass and evolutionary state. Component Aa2 in the close binary is relatively faint, but we think we have detected its spectral signature in the CCF of the difference spectrum that removes the flux of Aa1 (Fig. 2). If so, then our mass results are in broad agreement with the low mass models of the binary presented by Pablo et al. (2015) and with the Aa1 mass estimated from the observed apsidal motion and probable age (Benvenuto et al. 2002; Pablo et al. 2015). If the stars Aa1 and Aa2 are in synchronous rotation with the orbit (perhaps at periastron), then the ratio of radii should be similar to the ratio of $V \sin i$ values (Table 3), $R_2/R_1 \approx 0.28$. Thus, we expect that the flux ratio in the visible part of the spectrum will be

$$\frac{F_\lambda({\rm Aa2})}{F_\lambda({\rm Aa1})} = \frac{f_\lambda({\rm Aa2})}{f_\lambda({\rm Aa1})} \left(\frac{R_2}{R_1}\right)^2$$

or $F_\lambda({\rm Aa2})/F_\lambda({\rm Aa1}) = 0.04$ in the V-band for a surface flux ratio of $f_\lambda({\rm Aa2})/f_\lambda({\rm Aa1}) = 0.52$ from the TLUSTY models for the parameters given in Table 3. Detecting the spectrum of Aa2 is challenging, but because it may present lines that are much narrower than those of Aa1 and Ab, it may be possible to separate out all the components in high S/N spectroscopy. With the stellar parameters of Aa1 and Ab now better established, we can reliably predict how the blending influence of these components will appear in the composite line profiles.

By subtracting these components, the spectrum of Aa2 may be finally revealed, its radial velocity curve measured, and hence accurate masses determined.

We are grateful to Charles Proffitt and Denise Taylor of STScI for their aid in planning the observations with *HST*. We thank Brian Mason, William Hartkopf, and Andrei Tokovinin for information about their speckle observations of δ Ori, and we also thank Tomer Shenar for sharing results in advance of publication. Support for program #13450 was provided by NASA through a grant from the Space Telescope Science Institute, which is operated by the Association of Universities for Research in Astronomy, Inc., under NASA contract NAS 5-26555. NDR gratefully acknowledges his CRAQ (Québec) fellowship. AFJM is grateful for financial aid to NSERC (Canada) and FRQNT (Québec).

Facilities: HST

REFERENCES

Benvenuto, O. G., Serenelli, A. M., Althaus, L. G., Barbá, R. H., & Morrell, N. I. 2002, MNRAS, 330, 435

Biretta, J., Hernandez, S., Ely, J., et al. 2015, STIS Instrument Handbook, Version 14.0 (Baltimore: STScI)

Bostroem, K., & Proffitt, C. 2011, STIS Data Handbook, Version 6.0 (Baltimore: STScI)

Caballero, J. A., & Solano, E. 2008, A&A, 485, 931

Corcoran, M. F., Nichols, J. S., Pablo, H., et al. 2015, ApJ, in press

Harmanec, P., Mayer, P., & Šlechta, M. 2013, in Massive Stars: From Alpha to Omega (http://a2omega-conference.net/Posters/SessionII_19_Harmanec.pdf)

Harvey, A. S., Stickland, D. J., Howarth, I. D., & Zuiderwijk, E. J. 1987, Observatory, 107, 205

Harvin, J. A., Gies, D. R., Bagnuolo, W. G., Jr., Penny, L. R., & Thaller, M. L. 2002, ApJ, 565, 1216

Heap, S. R., Lanz, T., & Hubeny, I. 2006, ApJ, 638, 409

Kimble, R. A., Woodgate, B. E., Bowers, C. W., et al. 1998, ApJ, 492, L83

Koch, R. H., & Hrivnak, B. J. 1981, ApJ, 248, 249

Lanz, T., & Hubeny, I. 2003, ApJS, 146, 417

Lanz, T., & Hubeny, I. 2007, ApJS, 169, 83

Luyten, W. J., Struve, O., & Morgan, W. W. 1939, Publ. Yerkes Obs., 7, 251

Martins, F., Schaerer, D., & Hillier, D. J. 2005, A&A, 436, 1049

Mason, B. D., Hartkopf, W. I., Gies, D. R., Henry, T. J., & Helsel, J. W. 2009, AJ, 137, 3358

Mayer, P., Harmanec, P., Wolf, M., Božić, H., & Šlechta, M. 2010, A&A, 520, A89

Morbey, C. L., & Brosterhus, E. B. 1974, PASP, 86, 455

Nichols, J., Huenemoerder, D. P., Corcoran, M. F., et al. 2015, ApJ, submitted

Pablo, H., Richardson, N. D., Moffat, A. F. J., et al. 2015, ApJ, in press (arXiv:1504.08002)

Shenar, T., Oskinova, L., Hamann, W.-R., et al. 2015, ApJ, in press (arXiv:1503.03476)

Sota, A., Maíz Apellániz, J., Walborn, N. R., et al. 2011, ApJS, 193, 24

Tokovinin, A., Mason, B. D., & Hartkopf, W. I. 2014, AJ, 147, 123

Torres, G., Andersen, J., & Giménez, A. 2010, A&ARv, 18, 67

Wade, R. A., & Rucinski, S. M. 1985, A&AS, 60, 471

Zucker, S. 2003, MNRAS, 342, 1291

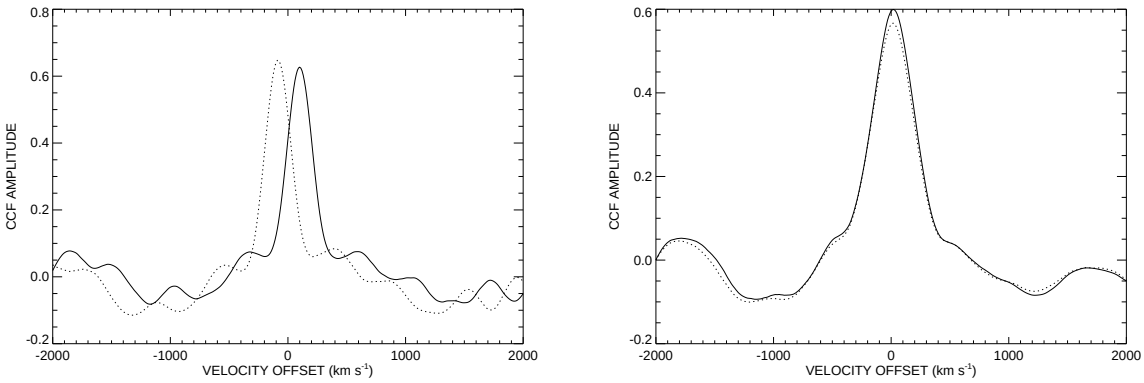

Fig. 1.— The cross-correlation functions for δ Ori Aa1 (left) and δ Ori Ab (right). The solid and dotted lines show the results for the first and second STIS observation, respectively.

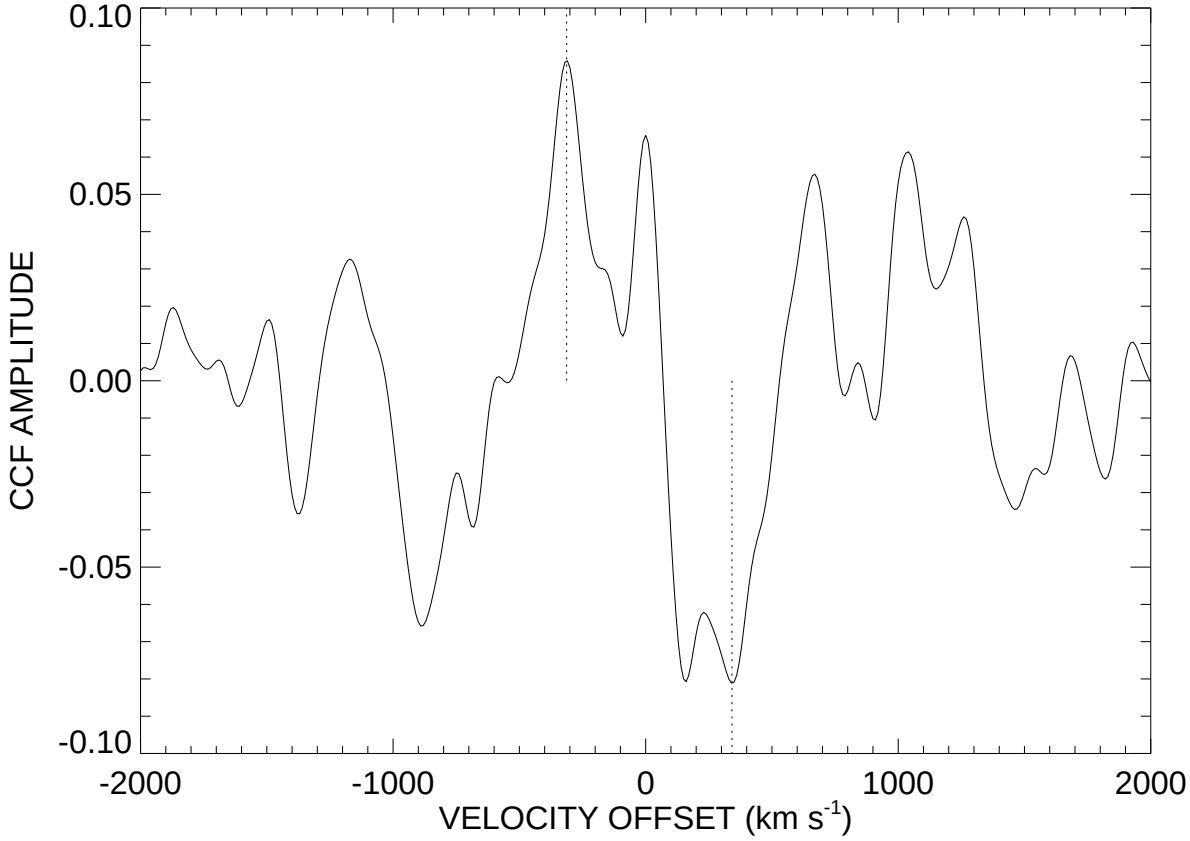

Fig. 2.— The cross-correlation function of the difference of the two δ Ori Aa spectra in the reference frame of component Aa1. A model spectrum for Aa2 was used as the template. The vertical dotted lines indicate the possible detection of Aa2 in the first (left) and second (right) observation. These velocity offsets correspond to the predicted shifts of Aa2 at the times of the observations.

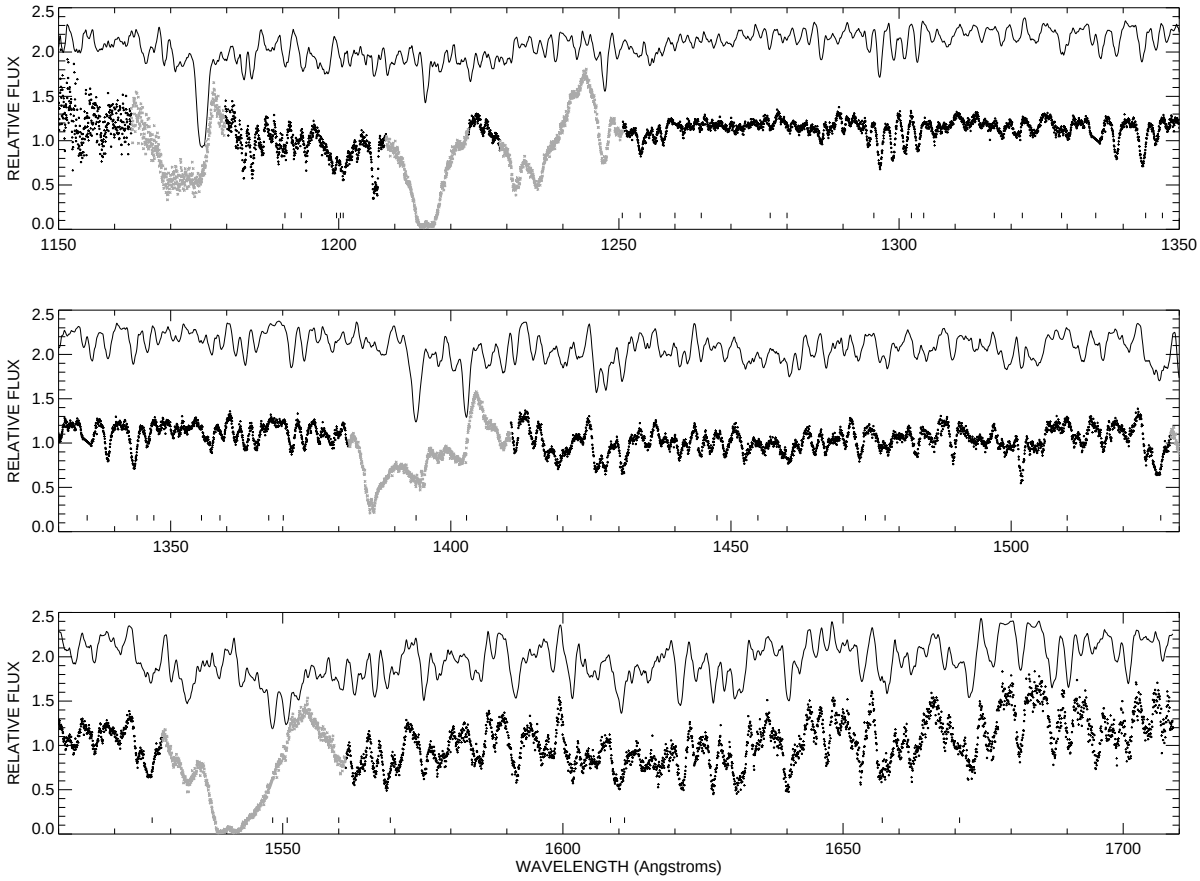

Fig. 3.— The normalized ultraviolet spectrum of δ Ori Aa1 (below) compared with a model from TLUSTY (solid line above, offset by 0.8 for clarity). The black plus signs indicate the result of shifting and adding the spectrum to the reference frame of Aa1, while the gray crosses show a simple average spectrum in the rest frame in the vicinity of the stellar wind lines. The lower line segments indicate the locations where interstellar lines were removed from the spectrum.

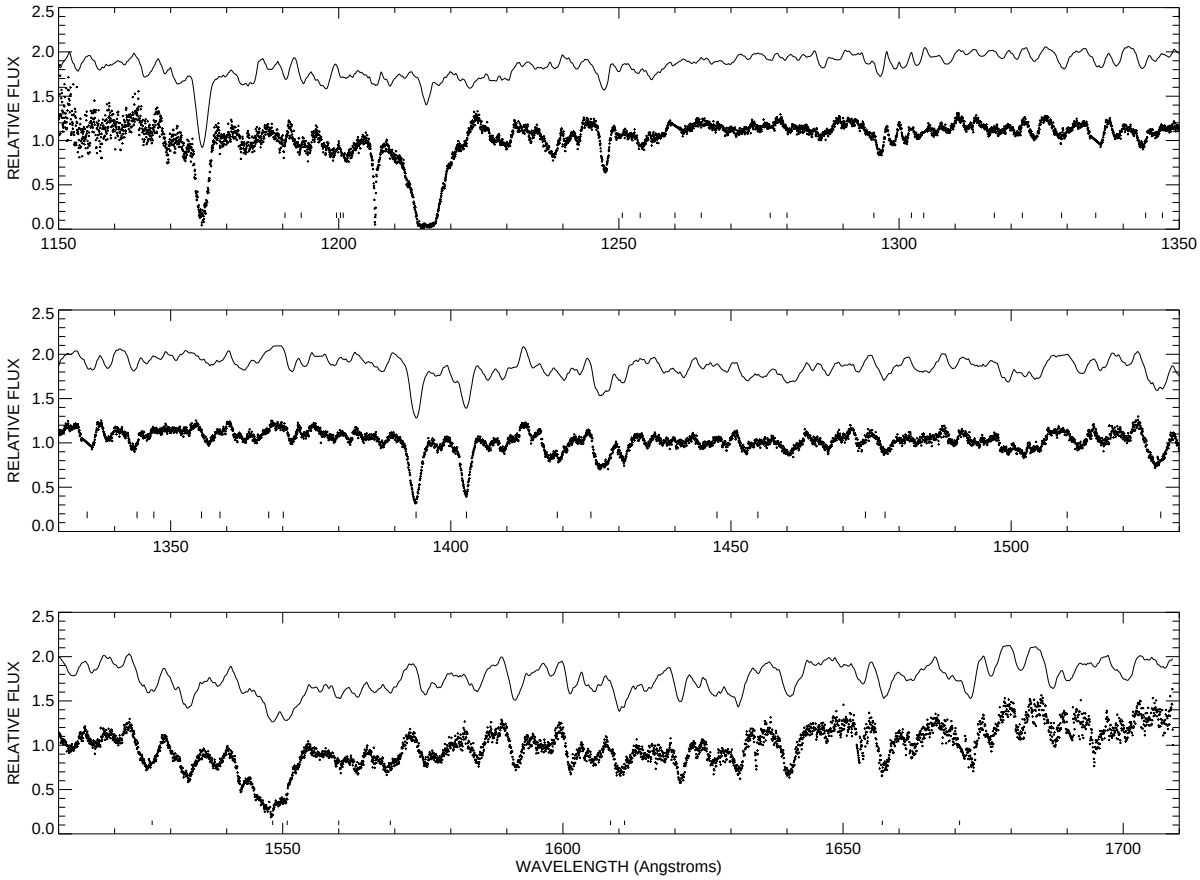

Fig. 4.— The normalized ultraviolet spectrum of δ Ori Ab (plus signs) compared with a model from TLUSTY (solid line, offset by 0.8 for clarity) in the same format as Figure 3.

Table 1. Radial Velocity Measurements

System Component	Date (HJD–2,400,000)	Orbital Phase	V_r (km s^{-1})	σ (km s^{-1})
Aa1	57022.1644	0.725	99.5	1.6
Aa1	57064.0356	0.029	−85.0	1.5
Aa2	57022.1644	0.725	−213.3	20.0
Aa2	57064.0356	0.029	256.7	20.0
Ab	57022.1757	···	19.1	2.7
Ab	57064.0764	···	15.9	2.9

Table 2. Orbital Elements for δ Ori Aa

Element	Value
P (days)	5.732436[a]
T (HJD–2,400,000)	57040.938[b]
e	0.1124[b]
ω (deg)	144.2[b]
K_1 (km s^{-1})	104.6 ± 1.6
K_2 (km s^{-1})	266 ± 20
γ_1 (km s^{-1})	21.1 ± 1.6
γ_2 (km s^{-1})	-14 ± 20
M_1 ($M_\odot$)	23.3 ± 3.1[c]
M_2 ($M_\odot$)	9.1 ± 1.0[c]
a ($R_\odot$)	43.0 ± 2.4[c]

[a]Fixed with the value from Mayer et al. (2010).

[b]Fixed with values from Pablo et al. (2015).

[c]For $i = 76\overset{\circ}{.}4$ from Pablo et al. (2015).

Table 3. Stellar Parameters for δ Ori A

Parameter	Aa1	Aa2	Ab
$T_{\rm eff}$ (kK)	30.9 ± 1.8	≈ 23	31.3 ± 1.7
$\log g$ (cgs)	3.37[a]	4.0	3.5[a]
$V \sin i$ (km s^{-1})	144 ± 8	≈ 40	252 ± 13
M ($M_\odot$)	23.3 ± 3.1	9.1 ± 1.0	···

[a]Fixed with values from Shenar et al. (2015).